

## Article

# Topographical Impact on Snow Cover Distribution in the Trans-Himalayan Region of Ladakh, India

Stanzin Passang <sup>1</sup>,  Susanne Schmidt <sup>1</sup>,  and Marcus Nüsser <sup>1,2,\*</sup>, <sup>1</sup> Department of Geography, South Asia Institute, Heidelberg University, 69115 Heidelberg, Germany<sup>2</sup> Heidelberg Center for the Environment, Heidelberg University, 69120 Heidelberg, Germany

\* Correspondence: marcus.nuesser@uni-heidelberg.de

**Abstract:** This article presents the distribution of seasonal snow cover in the Trans-Himalayan region of Ladakh over the observation period of 2000–2019. Seasonal snow cover area and duration have been monitored and mapped based on the MODIS Normalised Difference Snow Index (NDSI). Using different MODIS cloud removal algorithms, monthly mean cloud-covered areas have been reduced to 3%. Pixel-wise approaches using Mann–Kendall (MK) and Sen’s slope trend tests allow to assess seasonal and annual trends of snow cover days (SCD) and snow cover area (SCA) across seven delineated subregions of Ladakh. Analyses include the impact of topographical parameters (elevation, slope, aspect). Overall, the mean annual SCA amounts to 42%, varying from 15% in August to 71% in February. However, large differences of SCA have been detected between and within subregions. The trend analysis of SCA shows a non-significant, slight increase for summer as well as for the entire year and a decrease for spring and winter seasons. The SCD trend analysis indicates more pixels with a significant increase than a decrease. In total, 12% of all pixels show an increasing trend in summer, 6% over the entire year, 3% in autumn, and 2% in spring and winter, whereas less than 2% of all pixels show a decreasing trend in all seasons. The results are important for regional irrigated agricultural production and freshwater supply in the context of climate change.

**Keywords:** snow cover; terrestrial photography; MODIS; snow cover trends; Ladakh; Trans-Himalaya; India



**Citation:** Passang, S.; Schmidt, S.; Nüsser, M. Topographical Impact on Snow Cover Distribution in the Trans-Himalayan Region of Ladakh, India. *Geosciences* **2022**, *12*, 311. <https://doi.org/10.3390/geosciences12080311>

Academic Editors: Jesus Martinez-Frias, Ulrich Kamp, Dmitry Ganyushkin and Bijeeesh Kozhikkodan Veettil

Received: 15 July 2022

Accepted: 18 August 2022

Published: 20 August 2022

**Publisher’s Note:** MDPI stays neutral with regard to jurisdictional claims in published maps and institutional affiliations.



**Copyright:** © 2022 by the authors. Licensee MDPI, Basel, Switzerland. This article is an open access article distributed under the terms and conditions of the Creative Commons Attribution (CC BY) license (<https://creativecommons.org/licenses/by/4.0/>).

## 1. Introduction

Seasonal snow cover and glaciers are key components of the Himalayan hydrological cycle, as more than 60% of the annual discharge is supplied by meltwater, with considerable variation across the region [1–5]. Especially in the cold-arid Trans-Himalayan region of Ladakh, meltwater supply from the cryosphere is of utmost importance for irrigated agriculture in spring and summer, when water demand is highest [6,7]. Thus, detailed information on snow-covered areas is essential for integrated water resource management and for assessments of regional climate change and associated impacts on meltwater runoff [8,9]. To address these crucial aspects, mapping and monitoring of spatial and temporal snow cover dynamics are urgently needed to support cryosphere-dependent livelihoods [10]. Despite the importance of seasonal snow cover for irrigated land use, the amount and timing of high-altitude snowfall is largely unknown [11]. Only few studies have analysed the distribution, duration, and trends of seasonal snow cover on the Himalayan scale [12–15]. To quantify snow-covered area (SCA) and snow cover days (SCD) at the regional scale across High-Mountain Asia [2,3,16–20], different snow products of Moderate-Resolution Imaging Spectroradiometer (MODIS) have been used, including the 8-day global-gridded product with a spatial resolution of 0.05° [13] or daily snow products with a spatial resolution of 500 m [12,14,20,21]. However, enormous interregional differences and large variabilities make it difficult to assess snow cover distribution and trends for the entire Himalayan region [12,13]. Therefore, detailed studies are required

for an improved understanding of snow cover distribution and related changes. On the regional scale, the snow cover pattern is influenced by elevation and other topographical parameters such as aspect and slope [22,23]. Only few studies consider these topographic controls on snow cover distribution in the Himalayas [3,21,24]. For the Trans-Himalayan region of Ladakh, seasonal snow cover dynamics and their changes are largely unknown as long-term snow observations are only available for the meteorological station in Leh (Figure 1). Using climatological reanalysis data, the spatial distribution of solid and liquid precipitation can be assessed without considering the impact of topography [25].

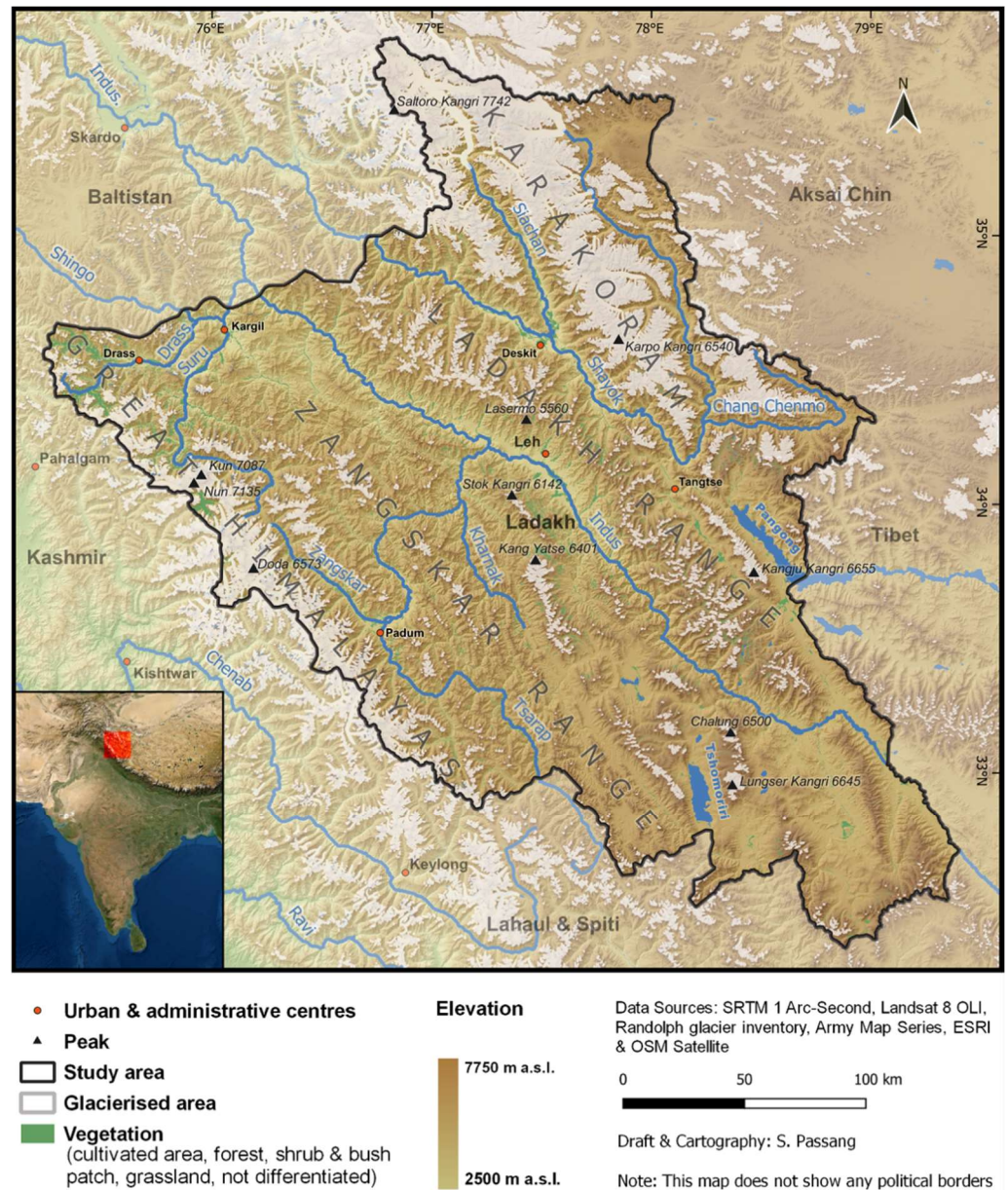


**Figure 1.** The Trans-Himalayan region of Ladakh, sandwiched between the Greater Himalayas, the Karakoram, and the Tibetan plateau. Place names follow the spelling in Ladakhi language [26], e.g., Zangskar (Zanskar), Tshomoriri (Tso Moriri), and Siachan (Siachen).

Against the background of these knowledge gaps, this article provides an analysis of snow cover distribution and duration in Ladakh using daily MODIS snow product data for the period of 2000–2019. The spatio-temporal patterns and trends of snow-covered area (SCA) and snow cover days (SCD) have been investigated in seven delineated subregions, based on watersheds and mountain ranges. Furthermore, the impact of topography (ele-

vation, slope, and aspect) on the SCA has been analysed to detect and quantify trends in individual subregions.

Ladakh is located in the rain shadow of the Karakoram to the north and the Greater Himalaya to the south. Due to the cold-arid conditions along the western edge of the Tibetan plateau, only small high-altitude glaciers exist along the Central Ladakh Range and on the Changthang Plateau [27–30], whereas large valley glaciers exist in the Karakoram [31,32] and along the Greater Himalayan Range [33]. In the winters, large *aufeis* fields occur along the tributaries of the Upper Indus Basin (UIB) and in the endorheic basins of Tshomoriri and Pangong as a temporary cryosphere component [34].

The elevation ranges from 2540 m a.s.l. in the lower Indus Valley near Kargil in western Ladakh to 7742 m a.s.l. on the Saltoro Ridge in the north (Figure 1). The mean elevation of Ladakh amounts to 4875 m a.s.l., increasing from the west to the east (Figure 2, Table 1); thus, the subregion Suru has the lowest and Pangong the highest mean elevation. Temperatures vary between more than 30 °C in the lower Indus valley during summer to less than −40 °C during winter in Drass of the Suru region. The region receives low precipitation, which decreases from the west to the east from about 600 mm to less than 100 mm in the Indus valley and in the Changthang region [25,35].

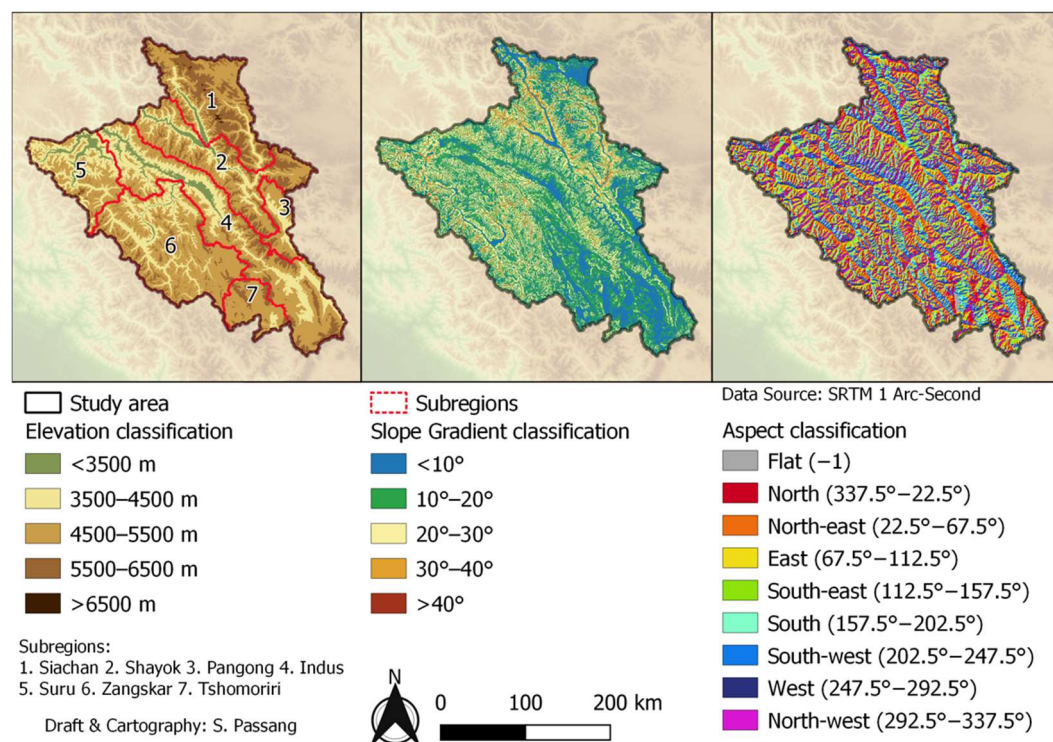


**Figure 2.** Topographical parameters (spatial resolution of 500 m) of the study area (75°32′ E, 35°67′ N to 79°46′ E, 32°34′ N): elevation (**left**), slope (**middle**), and aspect (**right**) (Table 1).

**Table 1.** Spatial distribution of elevation, slope, and aspect in the seven subregions of Ladakh.

	Siachan (Siachen)		Shayok (Shyok)		Pangong		Indus		Suru		Zangskar (Zaskar)		Tshomoriri (Tso Moriri)	
	km <sup>2</sup>	%	km <sup>2</sup>	%	km <sup>2</sup>	%	km <sup>2</sup>	%	km <sup>2</sup>	%	km <sup>2</sup>	%	km <sup>2</sup>	%
Elevation (m a.s.l.)														
<3500	263	3	512	5	-	-	1067	6	740	11	157	1	-	-
3500–4500	845	8	1808	17	546	21	5476	32	2946	42	3365	23	132	4
4500–5500	4898	47	5638	53	1383	54	8297	48	3122	45	9872	67	2441	73
5500–6500	4333	41	2622	25	614	24	2293	13	148	2	1298	9	749	23
>6500	115	1	1	0	-	-	1	0	4	0	0	0	1	0

Table 1. Cont.

	Siachan (Siachen)		Shayok (Shyok)		Pangong		Indus		Suru		Zangskar (Zanskar)		Tshomoriri (Tso Moriri)	
	km <sup>2</sup>	%	km <sup>2</sup>	%	km <sup>2</sup>	%	km <sup>2</sup>	%	km <sup>2</sup>	%	km <sup>2</sup>	%	km <sup>2</sup>	%
Slope (°)														
<10	3216	31	2202	21	1090	43	5618	33	1118	16	3122	21	1633	49
10–20	3346	32	3975	38	1060	42	7616	44	2692	39	6075	41	1377	41
20–30	2595	25	3419	32	370	15	3565	21	2468	36	4575	31	303	9
30–40	1176	11	929	9	23	1	333	2	600	9	886	6	10	0
>40	119	1	54	1	-	-	2	0	37	1	34	0	-	-
Aspect														
N	1232	12	1285	12	231	9	2076	12	959	14	1593	11	320	10
NE	1560	15	1473	14	445	17	2566	15	865	13	2177	15	427	13
E	1348	13	1556	15	369	14	2217	13	865	13	2048	14	445	13
SE	1247	12	1188	11	295	12	1942	11	785	11	1639	11	328	10
S	1410	13	1112	11	224	9	1890	11	799	12	1533	10	371	11
SW	1490	14	1260	12	333	13	2374	14	820	12	1971	13	490	15
W	1134	11	1385	13	299	12	2240	13	877	13	1993	14	463	14
NW	1034	10	1316	12	236	9	1834	11	945	14	1739	12	381	11

## 2. Materials and Methods

### 2.1. Materials

Daily snow cover maps from MOD10A1 (MODIS Terra) and MYD10A1 (MODIS Aqua) with a resolution of 500 m were used to investigate the temporal and spatial distribution of seasonal SCA and SCD between October 2000 and September 2019. For the period from October 2000 to December 2016, binary snow cover data of MODIS Collection 5 were used, which are based on a global Normalised Difference Snow Index (NDSI) threshold of 0.4 [36]. For the period from January 2017 to September 2019, NDSI data from MODIS Collection 6 were used, as binary snow cover data are no longer available. These data were downloaded from the NASA Distributed Active Archive Center (DAAC), hosted by the National Snow and Ice Data Center (NSIDC) (<https://nsidc.org>; accessed on 22 November 2019). To validate the MODIS NDSI threshold, Landsat-8 OLI data (downloaded from <https://earthexplorer.usgs.gov>; accessed on 10 January 2020) and oblique terrestrial photographs from two permanently installed cameras mounted in the Leh valley between 3660 and 4900 m a.s.l. were used (Figure 3).

To analyse the impact of topographical parameters (elevation, slope, and aspect) on snow cover distribution, a void-filled Shuttle Radar Topography Mission Digital Elevation Model (SRTM-DEM) (<https://earthexplorer.usgs.gov>; accessed on 1 July 2019) was resampled to 500 m. To consider the spatial differentiation of climatic and topographical conditions, the study area was separated into seven subregions based on watersheds and mountain ranges: Siachan (Siachen), Shayok (Shyok), Pangong, Indus, Suru, Zangskar (Zanskar), and Tshomoriri (Tso Moriri) (Figure 2). DEMs with high spatial resolution (High-Mountain Asia (HMA) DEM [37] (retrieved from <https://nsidc.org>; accessed on 15 August 2020) and TanDEM-X 12 m data (retrieved on special request by German Aerospace Center (DLR)) were used to geo-reference terrestrial photographs, calculate viewsheds, and to delineate snow lines at the local scale using the Monoplotting Tool (MPT 2.0, Monoplotting Tool—WSL) as an additional ground truthing method (Figure 3).

### 2.2. Methods

To map and analyse SCD and SCA, daily cloud-free MODIS snow maps have been generated. Based on these data, monthly, seasonal, and annual composites have been calculated for the analysis of spatial and temporal distribution of SCA and the impact of topography on it. In a second step, trend analyses have been carried out for the SCA and SCD.

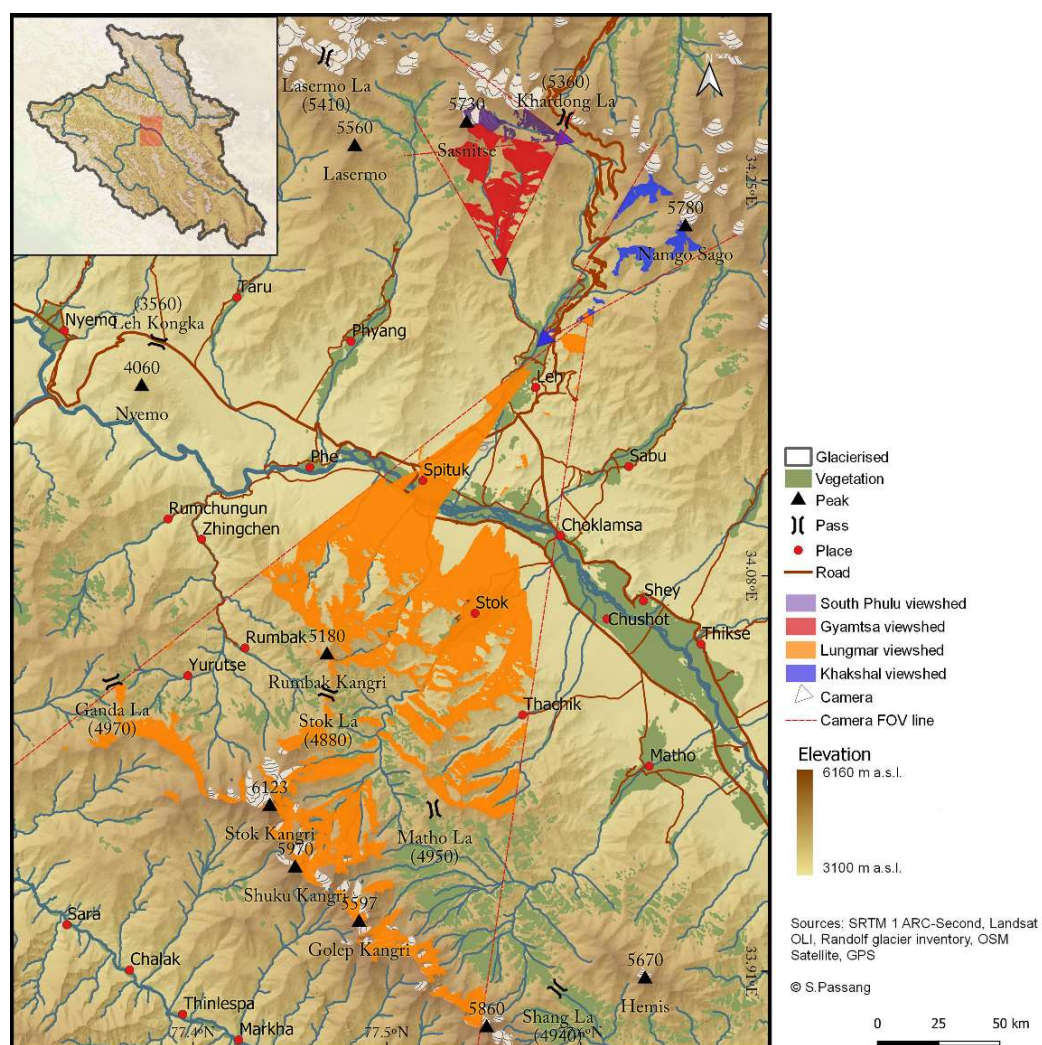


**Figure 3.** Locations and viewsheds of four terrestrial cameras. Gyamtsa (red) and Lungmar (orange) were used for MODIS validation in the present study.

### 2.2.1. NDSI Threshold Value Calibration

The binary data of global MODIS snow cover products were calculated based on the NDSI (Equation (1)) with a threshold of 0.4, for pixels with the visible reflectance (near infrared (NIR): Band 2) greater than 0.11 and Band 4 (green) reflectance greater than 0.10 [36]. In collection 5, the NDSI is calculated for MODIS Terra using green (Band 4) and shortwave infrared 1 (SWIR 1: Band 6), and for MODIS Aqua using green and SWIR 2 (Band 7) due to non-functional detectors. In collection 6, the quantitative image restoration (QIR) algorithm enables the usages of SWIR 1 for both Terra and Aqua with a higher accuracy compared to the usage of SWIR 2 [38]. Thus, for both MODIS Terra and Aqua, the NDSI can be calculated with the same band combinations (Equation (1)):

$$\text{NDSI} = (\text{Green} - \text{SWIR 1}) / (\text{Green} + \text{SWIR 1}) \quad (1)$$

The comparison of MODIS snow products collection 5 and 6 using different NDSI threshold schemes showed no significant differences and had identical accuracies [39]. Several studies, e.g., [12,40,41], applied the global reference NDSI threshold of 0.4 for the Himalaya and the Zangskar region [42], whereas in other studies a much lower threshold of 0.01 or 0.2 was suggested [39,43]. To enable statistical trend analyses, the same global reference NDSI threshold of 0.4, applied in the binary data of collection 5, was also used for collection 6.

To validate the NDSI threshold, two cloud-free Landsat-8 OLI tiles (path 147/row 36–37) from four seasons were used for ground truthing [44–47]. Pixels were classified as snow-covered if the NDSI was greater than or equal to 0.40 and the NIR was greater than 0.11 [44,48–50]. The snow cover data were resampled to 500 m to match the spatial resolution of MODIS.

An accuracy assessment was carried out using Cohen's kappa coefficient ( $\kappa$ ) method on a range of different MODIS NDSI threshold value images. The highest  $\kappa$  for each MODIS threshold value image was regarded to feature the appropriate NDSI threshold value, since  $\kappa$  represents the level of agreement between two datasets, considering the possibility of the agreement occurring by chance [51]. The formula is presented in Equation (2):

$$\kappa = \frac{p_o - p_e}{1 - p_e} \quad (2)$$

where  $p_o$  is the relative observed agreement among rates and  $p_e$  is the hypothetical probability of chance agreement.

The validation shows that the NDSI threshold varies between the seasons. In winter and spring, the NDSI predominantly exceeds the reference threshold value of 0.4, whereas in summer and autumn, the threshold is lower. However, the used NDSI threshold of 0.4, which also represents the global NDSI threshold, shows an overall accuracy of 87.20%.

In a second approach, Landsat-8 OLI and MODIS snow cover maps were compared to the monoplotted terrestrial images taken on the same date.

The results fit well with the terrestrial photos. Comparison amongst the coarse MODIS, high Landsat, and very high terrestrial photos shows that the resolution of pixels plays a huge role in detecting shallow and fragmented snow trace in the transition zone. MODIS underestimates the snow-covered area where a pixel is less than 50% snow-covered, and overestimates where a pixel is more than 50% snow-covered [52]. For example, ephemeral shallow and fragment snow pixels in the near range of the Lungmar camera are not registered by MODIS (Figure 4i), but are detected by Landsat (Figure 4h), and the permanent SCA is overestimated by MODIS where a pixel is more than 50% snow-covered (Figure 4l), compared to Landsat (Figure 4k). A slight underestimation of the snow cover can be assumed due to the shallow occurrence and patchy distribution of snow in the study area.

### 2.2.2. Methods Applied for MODIS Cloud Removal

Trend analyses of seasonal snow cover require high temporal resolution data. As in optical satellite data, clouds obscure the view on the ground, several approaches have been developed to reduce the degree of cloud-covered pixels in daily MODIS snow products [14,46,53–55]. Despite the cold-arid conditions of Ladakh, the mean cloud coverage amounts to 49.54% (Terra) and 55.36% (Aqua), varying from 11.80% (Terra) and 17.19% (Aqua) in October 2017 to 87.86% (Terra) and 90.29% (Aqua) in January 2008. Therefore, all daily MODIS snow products were processed to reduce the cloud pixels (Figure 5).

In the first step, pixel values of Terra and Aqua snow products in collection 5 were reclassified into three categories as snow (original snow and lake ice), land (no snow and lake classes), and clouds (all other missing/unusable classes). For collection 6, the NDSI was used to delineate between snow and land pixels. The ratios of land, snow, and cloud cover indicate the proportions of land, snow, and cloud-covered areas, respectively (Equation (3)):

$$R_C = \frac{A_C}{A} \times 100\% = \frac{P^X}{P} \times 100\% \quad (3)$$

where  $R_C$  is the ratio of land, snow, or cloud cover,  $A_C$  is the area of land, snow, or cloud cover,  $A$  is the total area of the study area,  $P^X$  is the number of land, snow, or cloud pixels, and  $P$  is the total number of pixels of the entire study area.

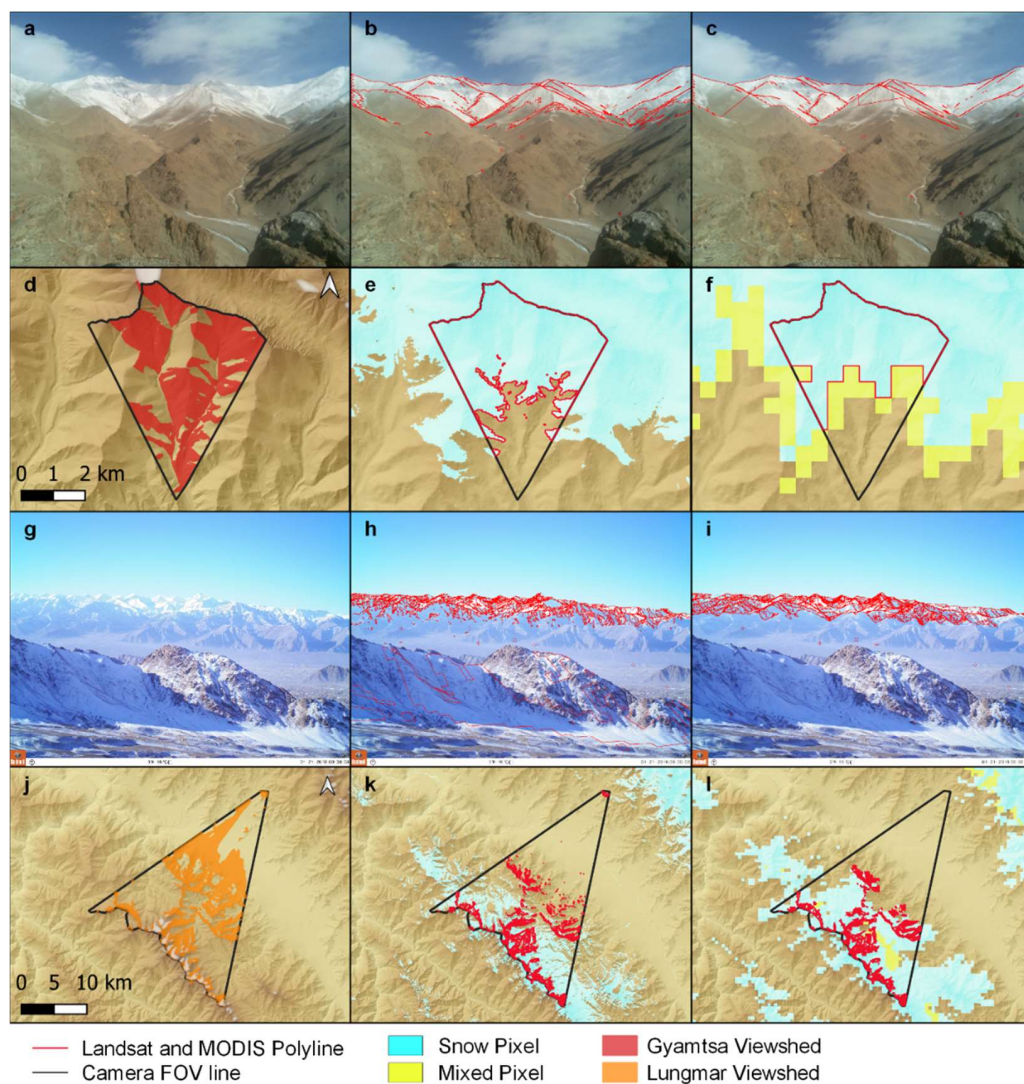


**Figure 4.** Terrestrial photograph taken from Gyamtsa on 23 January 2017 (a), overlaid with snow polylines (red lines) and control points (red crosses) derived from Landsat-8 OLI image (b) and MODIS (c). Gyamtsa camera view shed in red colour (d). Landsat-8 OLI (e) and MODIS snow shown in cyan (f). Terrestrial photograph taken from Lungmar on 21 January 2016 (g), overlaid with snow polylines (red lines) derived from Landsat-8 OLI (h) and MODIS (i). Lungmar view shed in orange colour (j). Landsat-8 OLI (k) and MODIS snow (l).

The combination of Terra and Aqua data takes advantage of the three-hour interval time between two observations. The cloud movement enables to reduce cloud-covered pixels under the assumption that snow conditions remain essentially constant within three hours. If a pixel is classified as cloud on one image but is reliably classified as land or snow cover on the other, then the cloud-covered pixel is reclassified appropriately [53,55] (Equation (4)):

$$P_{(x,y,t)} = \max(P_{(x,y,t)}^T, P_{(x,y,t)}^A) \tag{4}$$

where  $x$  is the latitude,  $y$  is the longitude, and  $t$  is a temporal (day) pixel,  $P$ .  $P^T$  and  $P^A$  represent pixels from Terra and Aqua, respectively.

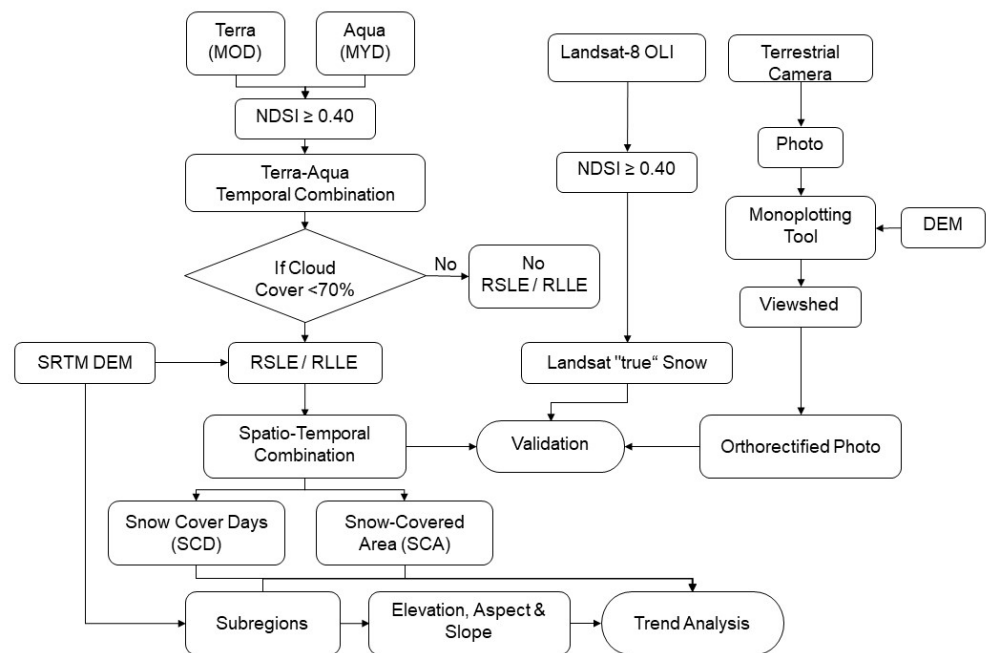


**Figure 5.** Flow chart of MODIS snow data processing validated with Landsat-8 imagery and orthorectified photos.

In the second step, a temporal combination was conducted which combines the preceding and succeeding day with the actual day of observation. Cloud-covered pixels are replaced either by snow or land pixels under the assumption of unchanged surface conditions within three days [46,55–57]. The formula is presented in Equation (5):

$$P_{(x,y,t)} = 1, \text{ if } (P_{(x,y,t-1)} = 1 \text{ and } P_{(x,y,t+1)} = 1) \tag{5}$$

where  $x$  is the latitude,  $y$  is the longitude, and  $t$  is a temporal (day) pixel,  $P$ .  $t - 1$  and  $t + 1$  represent the preceding and succeeding days, respectively, where 1 corresponds to snow cover and 0 for land cover.

The criterion of discarding images with more than 70% cloud pixels was applied before the third step to improve the results [58]. In total, 183 images were discarded over the entire observation period from October 2000 to September 2019. This approach contained an intermediate spatial step delineating the Regional Snow Line Elevation (RSLE) and the Regional Land Line Elevation (RLLE) by using the average (arithmetic mean) elevation derived from the SRTM DEM of all snow or land pixels of a single dataset [46,54,56,58–60] (Equations (6) and (7)):

$$RSLE = \frac{1}{n} \sum_{i=1}^n (P_{(x,y,z)}^S)_i \tag{6}$$

$$RLLE = \frac{1}{n} \sum_{i=1}^n (P_{(x,y,z)}^L)_i \tag{7}$$

where  $x$  is the latitude,  $y$  is the longitude, and  $z$  is the elevation of each snow pixel,  $PS$ , or land pixel,  $PL$ , in the list of elevations being averaged, and  $n$  is the total number of snow or land pixels.

Finally, cloud pixels were reclassified to land if their elevation value was below the mean RLLE, and to snow if their elevation value was above the mean RSLE (Figure 6). The remaining cloud pixels located in the transition zone between the RSLE and RLLE were assigned as mixed pixels (patches of snow and land) and not included in the analysis. The

result of this approach is a completely cloud-free spatio-temporal combination of MODIS data. The formula is presented in Equation (8):

$$P_{(x,y,z)}^C = \begin{cases} P_{(x,y,z)}^S & \text{if } (P_{(x,y,z)}^C > RSLE) \\ P_{(x,y,z)}^L & \text{if } (P_{(x,y,z)}^C > RLLE) \\ P_{(x,y,z)}^M & \text{if } (P_{(x,y,z)}^C \langle RSLE \text{ and } P_{(x,y,z)}^C \rangle RLLE) \end{cases} \quad (8)$$

where  $x$  is the latitude,  $y$  is the longitude, and  $z$  is the elevation value of a cloud ( $P^C$ ), snow ( $P^S$ ), land ( $P^L$ ), or mixed pixel ( $P^L$ ).

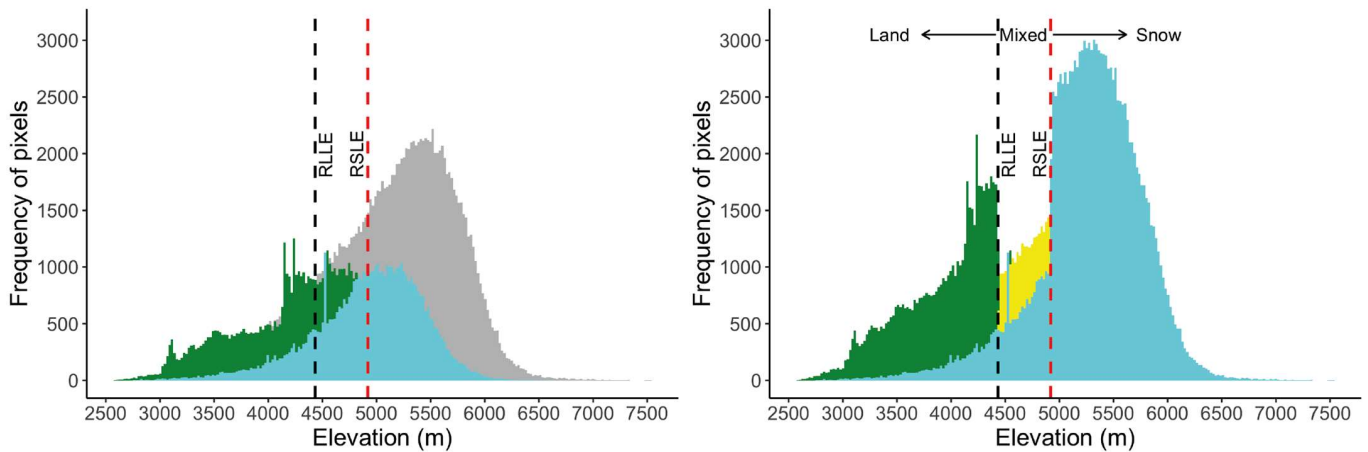


**Figure 6.** Number of land (green), snow (cyan), or cloud-covered (grey) pixels in relation to elevation (left) on a free temporal combination MODIS raster image on 16 January 2017. (Right): Spatio-temporal combination of MODIS image of 16 January 2017 after cloud reduction step 3. Cloud-covered pixels below RLLE (4433 m a.s.l.; black dashed line) are classified as land, between RSLE and RLLE (4919 m a.s.l.; red dashed line) as mixed pixels (yellow), and above RSLE as snow.

The first cloud reduction step (Figure 7), based on the combination of Terra and Aqua MODIS products, reduced the monthly mean cloud cover to 41%. The temporal combination approach decreased the cloud cover to 17%. With the final spatio-temporal combination, the remaining cloud pixels located between the RSLE and RLLE amounted to 3% on average (maximum 18%) and were classified as mixed pixels.

### 2.2.3. Snow Trend and Correlation Analysis

The monthly, seasonal, and annual mean MODIS SCA and SCD were calculated for the entire region of Ladakh and the seven subregions. To identify trends in time series, the Mann–Kendall (MK) [61,62] and Sen’s slope trend tests were applied [63]. The MK test is applied to identify whether there is a trend in the time series with statistical significance at the confidence interval of 90% ( $P < 0.1$ ), 95 % ( $p < 0.05$ ) and 99.9% ( $p < 0.01$ ). If a trend exists, the magnitude can be determined by the non-parametric Sen’s slope estimator, which is a robust method against outliers to estimate the slope of the trend. The trends were calculated for months, seasons, and hydrological years from 2000 to 2019. The values of the trend test and magnitude of trends are shown by Kendall’s tau ( $\tau$ ) coefficient and Sen’s slope (S). The seasons were categorized as autumn (September–November), winter (December–February), spring (March–May), and summer (June–August), and as the entire hydrological year (October–September).

A detailed study was conducted to analyse the spatio-temporal pattern and the impact of topographical parameters (elevation, aspect, and slope) on the SCA and its trends using the modified MK test with a two-variance correction approach [64,65]. A Sen’s slope trend test and a linear regression model were calculated to detect and quantify the magnitude of

trends across all subregions over 19 hydrological years (significance levels:  $p$ -values < 0.1, <0.05, and <0.01).

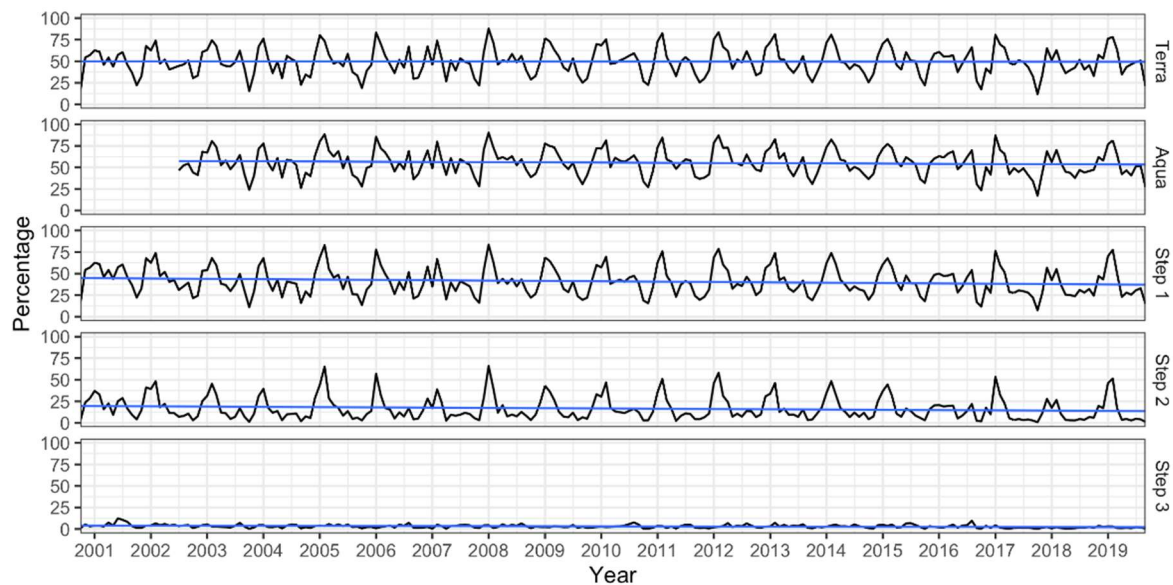


**Figure 7.** Monthly mean percentage of the cloud-covered pixels of MODIS daily snow product data featuring the reduction of cloud coverage (black line) and overall mean percentages (blue line) in three cloud reduction steps.

### 3. Results

Snow accumulation starts in September and lasts until February, when the maximum SCA of the entire area of Ladakh reaches 71%, with the exceptions of subregions Zangskar and Suru, where the maximum SCA is delayed until March (Figure 8, Table A2). An average of 61% of the study area is snow-covered during winter, varying from 49% in the snow-scarce winter of 2002/03 to 73% in the snowy winter of 2008/09. Three more snow-scarce winters occurred in 2000/01, 2011/12, and 2017/18, with a SCA of about 50%. In the year 2017/18, the SCA appeared to be significantly below average until summer. While the snow-scarce winter of 2002/03 was detectable in all subregions, the reduced snow cover during the winter of 2011/12 could only be identified in the two northern subregions of Siachan and Shayok, as well as in the south-eastern subregion of Zangskar. In winter of 2017/18, the reduction in snow cover could be detected in all subregions except Suru and Zangskar.

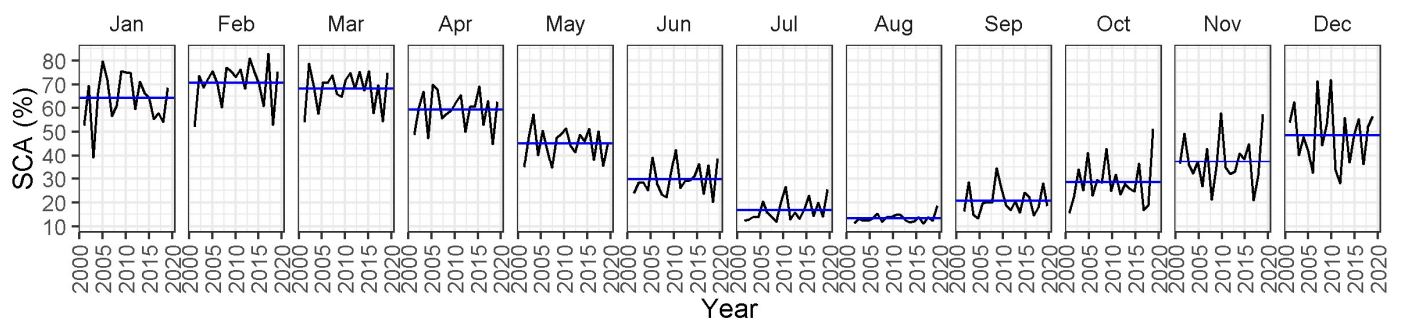


**Figure 8.** Monthly average percentages (black line) and overall monthly mean (blue line) of SCA for the entire study area of Ladakh over the period of 2000–2019.

In general, the winter SCA is generally characterized by high interannual variability, ranging from 28% to 72% in December and from 39% to 80% in January, while the SCA seems to be more stable in February, varying between 52% and 83%. About 10% of the entire study area is almost completely snow-free during winter (SCD less than 10 days in

winter), and these areas are located along the large valley bottoms of the Indus, Nubra, and Shayok rivers, as well as in the Changthang area of eastern Ladakh. Only minor differences can be detected between the SCA in winter and spring, when 46% of the region that is snow-covered in February is still snow-covered in March (Figure 9, top). Snow melt generally starts in April (Figure 8) and continues until August, when only 13% of the region is snow- or ice-covered. These permanently snow-covered areas are mainly located in the subregion of Siachan and along the Greater Himalayan range, the southern boundary of the study area (Figure 9, top). Depending on the SCA, the mean RSLE ascends from 4813 m a.s.l. in February to 5097 m a.s.l. in April, and to a maximum of 5560 m a.s.l. in August (Table A1).

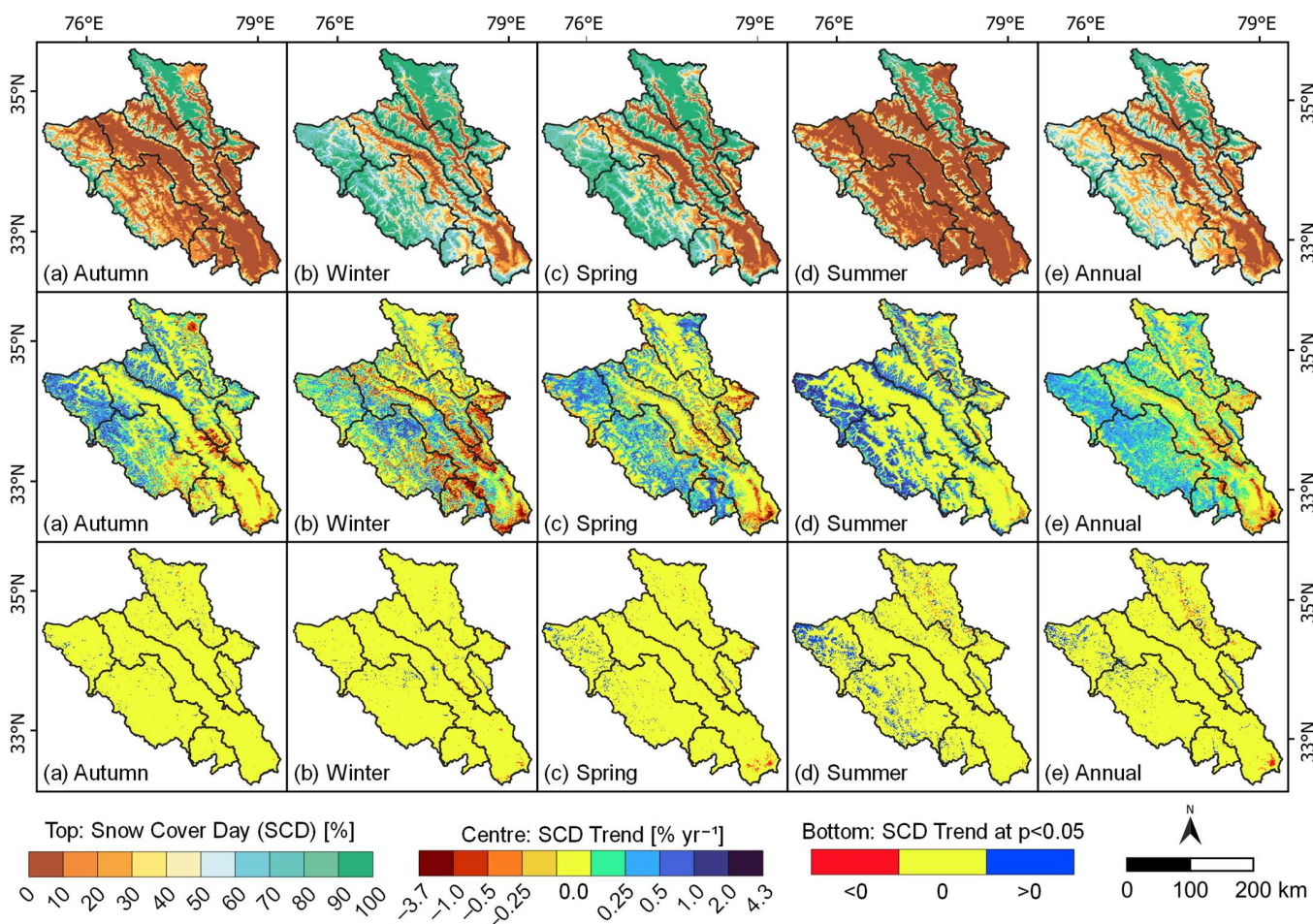


**Figure 9.** Pixel-wise analysis of snow cover days (SCD) for the entire study area of Ladakh over the period of 2000–2019. Mean seasonal and annual SCD (**top**), seasonal and annual trends of SCD (a) autumn: September–November, (b) winter: December–February, (c) spring: March–May, (d) summer: June–August, and (e) annual (hydrological year: October–September) (**centre**). SCD trends with significance level  $p < 0.1$ , yellow colour symbolizes no significant trend, red negative, and blue colour positive trends (**bottom**).

On the regional scale, the maximum winter SCAs with 79% and 75% can be detected in the subregions of Siachan and Suru, respectively, and the minimum in the Indus subregion, amounting to 41%. While in the Siachan subregion only minor interannual variations of the winter SCA can be identified, ranging between 70% and 85%, the largest differences can be identified for the Tshomoriri subregion, ranging between 34% and 78%. In most subregions, the snow melt starts in April, while in the two northern subregions, a delay of one month can be observed. The minimum SCA in summer amounts to less than 15% in all

subregions, with the exception of Siachan, where the SCA amounts to 42% and is larger than the mean winter SCA in the subregions of Indus and Pangong.

The SCA increases with elevation, where areas above 6500 m a.s.l. remain almost completely snow-covered throughout the year (Figure 10). In the subregions Siachan and Suru, more than 80% of the elevation zone of 5500–6500 m a.s.l. is snow-covered, with only slight seasonal variations, whereas in all other subregions, a characteristic seasonality of SCA can be observed ranging from 29% in summer to 70% in winter for the example of the Indus subregion. For the elevation zones of 4500–5500 m a.s.l. and below 4500 m a.s.l., this seasonality can be detected in all subregions where the SCA varies between 15% in summer and 64% in winter. Only in the Pangong subregion is this seasonality alleviated as the SCA in winter is less than 40%. Below the elevation zone of 3500–4500 m a.s.l., the winter snow covers less than 20% in the four northern subregions, while it reaches up to 60% in Suru and 40% in Zangskar.

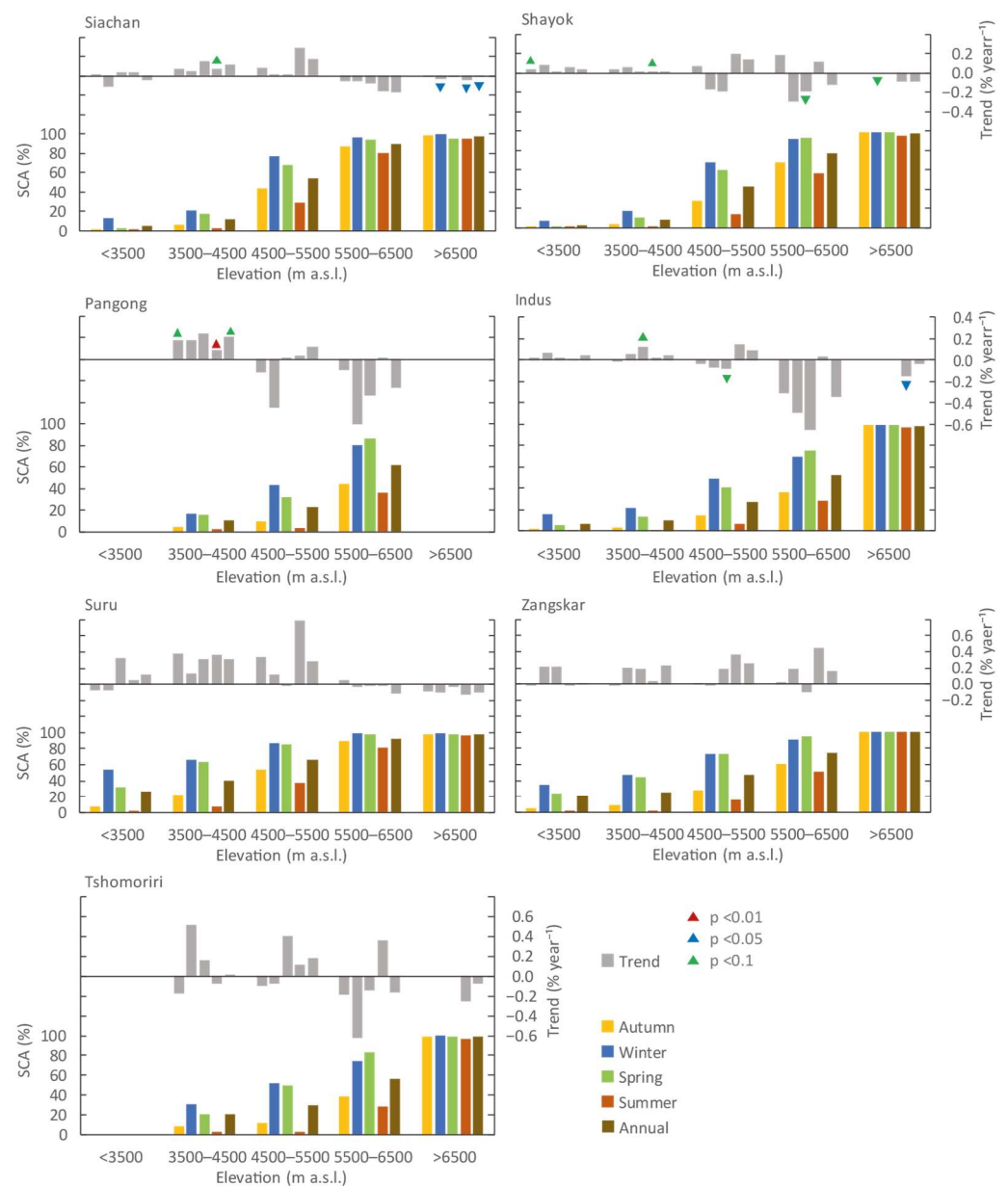


**Figure 10.** Seasonal and annual MODIS SCA and trends in relation to elevation zones of all subregions of Ladakh for the observation period of 2000–2019. *p*-value significance levels are shown in red ( $p < 0.01$ ), blue ( $p < 0.05$ ), and green ( $p < 0.1$ ) triangles (see also Table A2).

Aspect is another striking feature of snow cover distribution (Figure 11). South- and southwest-facing slopes are less snow-covered than all other slopes, except in the subregion of Siachan, where a shift to southwest- and west-facing slopes can be observed. In the subregions of Suru, Siachan, and Zangskar, the negative deviation is most prominent in autumn. In contrast, north- and northwest-facing slopes show the highest positive deviation in almost all subregions, except for Shayok, where west- and northwest-facing slopes, and for Tshomoriri, where north- and northeast-facing slopes have the largest SCA. In contrast to elevation and aspect, SCA does not show large differences between individual slope classes, except for the Shayok region, where a decrease of SCA with the increasing slope angle can be detected (Figure 12).

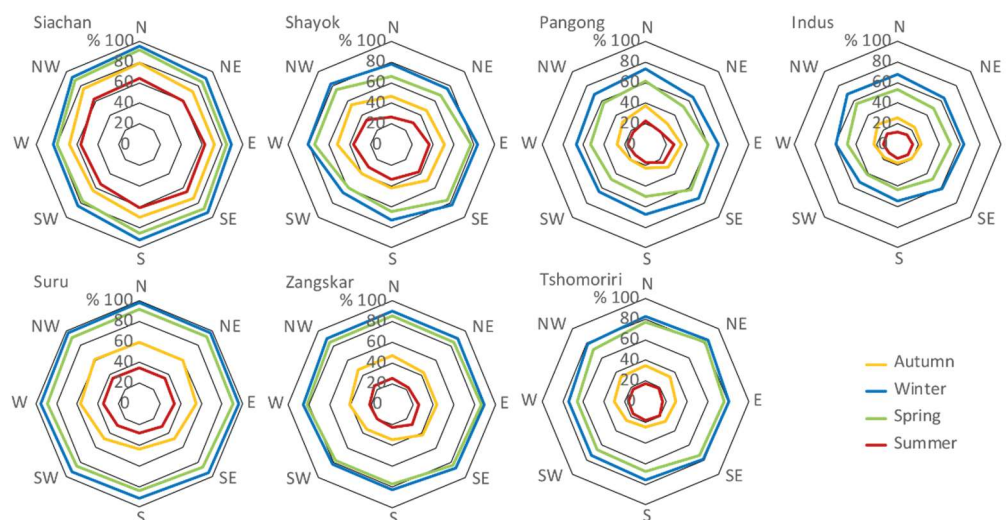


**Figure 11.** Seasonal MODIS SCA in relation to aspect across all subregions of the study area over the observation period of 2000–2019.

The trend analysis of the SCA for the entire study area shows no significant trends. However, a slight increase of the annual and summer SCA ( $0.08$  and  $0.2\%$  year<sup>-1</sup>) can be detected, while in winter and spring, a slight decrease can be identified (Table 2). The separated trend analysis of SCA on the regional scale shows slight, significant, increasing trends in the subregions of Suru ( $0.52\%$  year<sup>-1</sup>) and Zangskar ( $0.36\%$  year<sup>-1</sup>), while in the subregions of Siachan, Shayok, and Indus, a slight (non-significant) negative trend of SCA can be observed in spring. In general, the SCA trends show a non-significant heterogeneous pattern (Table A2).

In accordance with the SCA trend analysis, the pixel-wise analysis of SCD reveals a longer duration of snow coverage. However, only 6% of all pixels show a significant increasing trend and 2% of all pixels show a significant decreasing trend for the entire study area of Ladakh. Most pixels with a significant increasing trend in summer are located in the subregions of Suru and Zangskar, with 36% and 18% of all pixels, respectively. In general, this positive trend is also reflected by the trend analysis of the RSLE showing a downward shift for the entire region, which is significant for the months of June and July ( $-5.2$  and  $-5.6$  m year<sup>-1</sup>, respectively).

Most pixels with a decreasing trend are located in the eastern parts of Ladakh and more often in winter than in summer; for example, in the Pangong subregion, 5% show a decreasing trend in winter and only 1% in summer. In contrast, in the subregion of Siachan, most pixels with a negative trend are from summer (4%) (Figure 9, Table 3). This general negative trend of snow coverage in winter is also reflected in the RSLE, which shows an upward shift for the months of December and January.

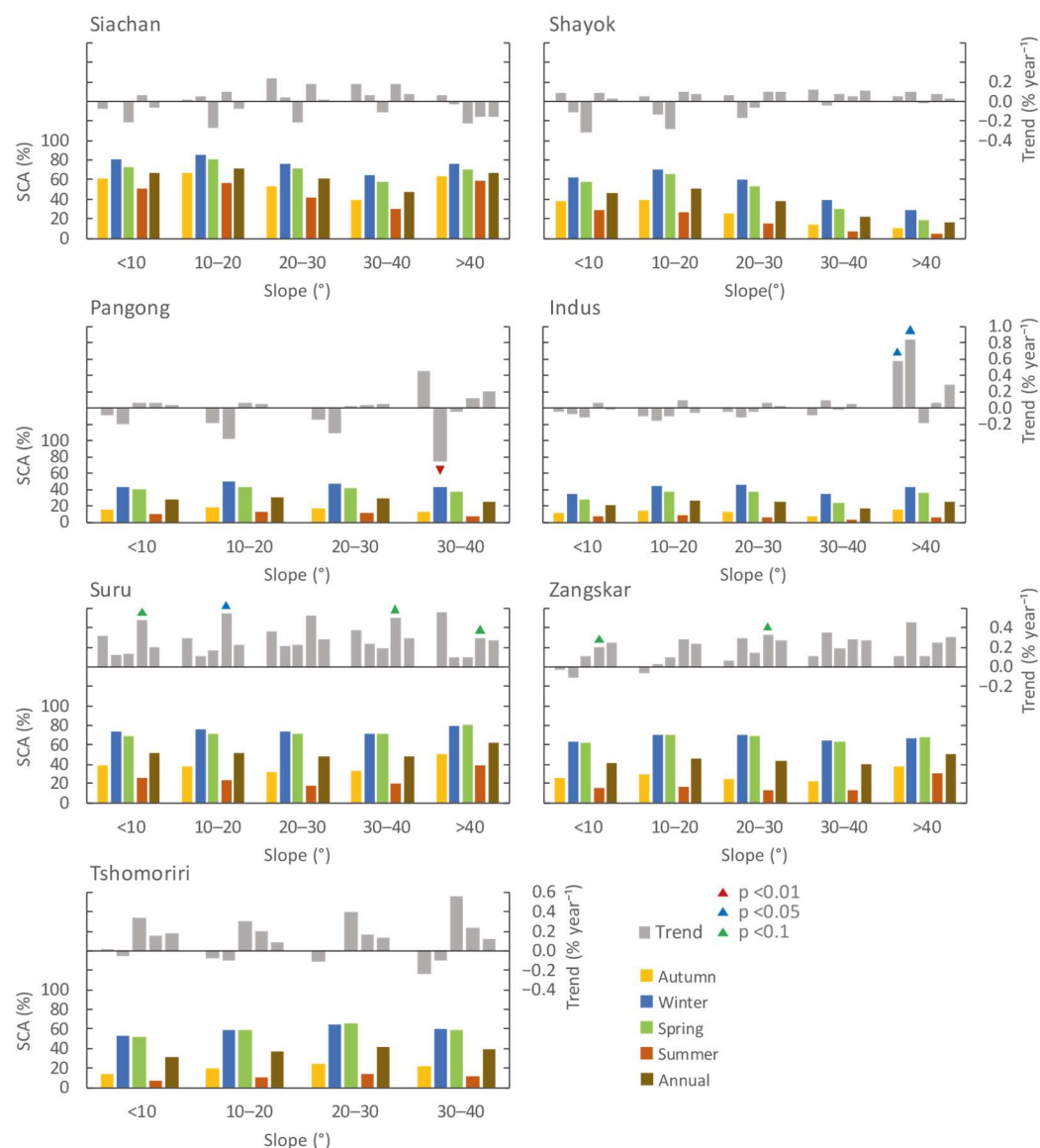


**Figure 12.** Seasonal and annual MODIS SCA and trends in relation to slope across all subregions over the observation period of 2000–2019.

**Table 2.** Annual and seasonal Mann–Kendall test statistics of the mean SCA (%) in the study area of Ladakh from 2000 to 2019.

	Linear Slope	Sen’s Slope	Z-Value	p-Value	Trend	Mean	SD
Annual	0.09	0.08	0.56	0.58	▲	41.85	4.32
Autumn	0.12	−0.01	0	1.00	▼	28.93	6.50
Winter	0.03	−0.10	−0.21	0.83	▼	61.17	6.49
Spring	−0.01	−0.07	−0.28	0.78	▼	57.53	6.33
Summer	0.22	0.20	0.98	0.33	▲	19.90	3.95

SD: Standard deviation, ▲: positive trend, ▼: negative trend.

The trend analysis of the SCA in relation to elevation shows a heterogeneous pattern. Slight decreasing trends can be detected above 5500 m a.s.l. in almost all subregions and are mostly significant above 6500 m a.s.l. In the elevation zone of 4500–5500 m a.s.l., an increasing trend of SCA can be observed in almost all subregions, which is highest in the southern subregions of Suru and Zangskar. In the north-eastern subregion of Pangong, a significant increasing trend of SCA can be identified for elevations below 4500 m a.s.l.

in autumn and summer (Figure 11). In all subregions except Zangskar and Tshomoriri, a significant increasing trend can be detected for the elevation zone of 3500–4500 m a.s.l. (Table A3) for the months of June and July.

**Table 3.** Increasing and decreasing trend of SCD in the study area of Ladakh from 2000 to 2019.

	Increasing Trend (Sen’s Slope > 0)							
	All		$p < 0.01$		$p < 0.05$		$p < 0.1$	
	km <sup>2</sup>	%	km <sup>2</sup>	%	km <sup>2</sup>	%	km <sup>2</sup>	%
Autumn	23,538.50	35.83	126.00	0.19	710.00	1.08	1571.00	2.39
Winter	21,587.75	32.86	103.75	0.16	559.50	0.85	1280.75	1.95
Spring	25,163.25	38.31	205.75	0.31	1011.00	1.54	1993.00	3.03
Summer	24,815.00	37.78	725.75	1.10	4269.00	6.50	7853.75	11.96
Annual	33,409.50	50.86	346.50	0.53	1934.75	2.95	4149.25	6.32
	Decreasing Trend (Sen’s Slope < 0)							
	All		$p < 0.01$		$p < 0.05$		$p < 0.1$	
	km <sup>2</sup>	%	km <sup>2</sup>	%	km <sup>2</sup>	%	km <sup>2</sup>	%
Autumn	9907.75	15.08	11.75	0.02	48.75	0.07	136.50	0.21
Winter	20,396.00	31.05	36.50	0.06	399.75	0.61	1027.25	1.56
Spring	12,440.50	18.94	47.75	0.07	365.00	0.56	811.25	1.23
Summer	3777.25	5.75	152.25	0.23	447.00	0.68	731.50	1.11
Annual	11,983.25	18.24	230.50	0.35	743.25	1.13	1220.00	1.86

*p*: Significance level.

#### 4. Discussion

The present study is based on daily MODIS snow cover data. Using a standardized global-NDSI threshold of 0.4 for MODIS snow products has shown an overall accuracy rate of about 87% compared to Landsat data, which is in line with other studies on snow cover mapping [20,46,55,56,66–68]. However, the dominant occurrence of snow cover in the Trans-Himalayan region of Ladakh consists of often shallow and fragmented snow traces and patches. This characteristic type of snow distribution creates difficulties in monitoring and change detection [66,69]. As small snow patches cannot be mapped with MODIS data, some studies have used Landsat data with a higher spatial but lower temporal resolution [70] or terrestrial cameras for continuous monitoring [22,71,72].

Comparing the SCA in Ladakh with adjoining parts of the South Asian Mountain Belt confirms the transitional position of the Trans-Himalayan region between the Karakoram and the Western Himalayas (Table 4). The Chandra basin in Himachal Pradesh (minimum elevation of 2800 m a.s.l.) is characterized by a snow cover of about 60% in August and of up to 99% in February [24]. In the Astore basin located to the east of the Nanga Parbat massif (minimum elevation of 1210 m a.s.l.), the SCA varies between 7% and up to 95% [73]. The study area of Ladakh is characterized by smaller differences in SCA, amounting to 15% in August and up to 71% in February, and the mean annual SCA of 42% is almost identical to the situation in the Chenab basin [2]. The average annual SCA value of 42% lies between average SCA values for the Karakoram range with 52% and the Western Himalayan range with 30% [12]. In another study [74], the SCA is estimated for the entire Upper Indus Basin (UIB) with a value of 21%, varying from 14% in the Shayok basin (including the upper watershed on the Tibetan Plateau) to 58% in the Shigar basin. On the regional scale, a decreasing SCA from west to east and from south to north is observed, which reflects the general precipitation gradient [11,75] and the influence of westerlies on solid precipitation in winter [76]. While the maximum SCA in the Astore basin is reached in January [73], in most subregions of Ladakh it occurs in February, except of Suru and Zangskar, where the maximum is not reached until March, which is similar to most parts of the neighbouring Gilgit Baltistan (March) [18] and Jhelum (February) [77]. Snow accumulation in Ladakh

starts in September, which is in accordance with observations from Gilgit Baltistan [18] and almost one month earlier than in the Karakoram, observed by Dharpure et al. [12].

**Table 4.** Selected studies focusing on snow cover distribution and trends in the high mountain regions of South Asia.

Region	Observation Period	SCA and Trends	Topics	Reference
UIB (Gilgit Baltistan)	2000–2017	Max: 86% in February/March, Min: 36% in August Slight non-significant increasing trend	Elevation zones	[18]
Chandra basin (Himachal Pradesh)	2001–2017	Max: 99% in February, Min: 60% in August	Elevation, slope, aspect	[24]
Chenab basin Satluj basin Ravi basin Beas basin (Himachal Pradesh)	2003–2004	42% mean annual 23% mean annual 33% mean annual 38% mean annual	Elevation, aspect	[2]
UIB	2001–2012	Annual SCA: non-significant, slightly decreasing trend for UIB and all subbasins, except Gilgit	Elevation, aspect, NAO	[74]
Jhelum and Kabul basins	2001–2012	Annual SCA: non-significant, slightly increasing trend for Jhelum and Kabul basins	Elevation, aspect, NAO	[74]
Astore basin (Gilgit Baltistan)	2000–2012	Max: 95% in January, Min: 7% in August stable (tends to slight increase) trend	Elevation zones	[73]
Karakoram (KK) Western Himalaya (WH) Central Himalaya (CH) Eastern Himalaya (EH) Karakoram-Himalaya (KH)	2000–2019	52% mean annual 31% mean annual 13% mean annual 10% mean annual 26% mean annual Non-significant, increasing trend for KK, WH, CH Non-significant, decreasing trend for EH, KH	Meteorological variables	[12]
Karakoram Western Himalaya Central Himalaya Eastern Himalaya Karakoram-Himalaya	2000–2008	52% mean annual 30% mean annual 12% mean annual 11% mean annual 26% mean annual Non-significant, increasing trend for all subregions and the entire KH	Meteorological variables	[12]
Karakoram Western Himalaya Central Himalaya Eastern Himalaya Karakoram-Himalaya	2008–2018	52% mean annual 31% mean annual 12% mean annual 10% mean annual 26% mean annual decreasing trend for all subregions and the entire KH, which is significant for WH and KH	Meteorological variables	[12]
UIB	2000–2008	negative trend for winter snow cover; no trend for all other seasons and the entire year	Elevation zones, runoff	[13]

The significant impact of aspect on SCA can be identified by the large differences between north-facing and south-facing slopes. As north-facing slopes receive less solar radiation, especially during autumn and winter, snow accumulation starts earlier, and snow melt commences later in comparison to south-facing slopes. These characteristic differences are most prominent in subtropical mountains [78].

A comparison of decadal snow cover trend analyses with studies from adjoining Himalayan regions is difficult, mainly due to differences in the length of the observation periods. Dharpure et al. have detected a non-significant, slightly increasing trend of SCA (0.21% year<sup>-1</sup>) along the entire Himalayan range between 2000 and 2008, which

reversed to a significant negative trend since 2008 ( $-0.42\%$  year<sup>-1</sup>). However, almost stable conditions have been identified over the entire observation period from 2000 to 2019 ( $0.00\%$  year<sup>-1</sup>) [12]. In the same study, non-significant positive trends of SCA have been observed for the Karakoram and Western Himalayas for 2000–2008, and a significant negative trend since 2008 [12]. In contrast, other studies have reported non-significant decreasing trends for the Upper Indus Basin over the periods 2001–2012 [74] and 2000–2008, respectively, which is significant in winter [13]. No clear trend of SCA can be identified for Ladakh, however the detected slight but non-significant increase of the annual and summer SCA can possibly be related to an increase in cloudburst events, as witnessed during several field visits.

Overall, a comparison of these studies underlines the relevance of regional analyses to capture spatio-temporal dynamics of seasonal snow cover. This is particularly important for cold-arid areas, where irrigation of agricultural fields solely depends on early melt water supply in spring [7,79]. In this context, local and subregional studies of snow cover distribution and duration are of utmost importance for livelihoods and development in Ladakh and neighbouring regions.

## 5. Conclusions

Similar to the adjoining mountain regions, components of the cryosphere are of vital importance for downstream settlements and irrigated agriculture in Trans-Himalayan regions. This study showed the potential of combining terrestrial photography with satellite imagery to obtain more accurate and detailed information on seasonal snow cover distribution and duration across various scales. The results revealed a high variability in seasonal snow cover across the seven different subregions and over the observation period of almost twenty years. For an improved understanding of spatial and temporal dynamics of regional snow cover distribution and duration, terrestrial data and satellite imagery with high spatial and high temporal resolution should be combined for any hydrological and development studies in the context of climate change.

**Author Contributions:** Conceptualization, M.N., S.S., and S.P.; methodology, S.P. and S.S.; validation, S.P.; formal analysis, S.P.; investigation, S.P.; resources, S.P.; data curation, S.P.; writing—original draft preparation, S.P., S.S., and M.N.; writing—review and editing, M.N. and S.S.; visualization, S.P.; supervision, M.N.; project administration, M.N.; funding acquisition, M.N. All authors have read and agreed to the published version of the manuscript.

**Funding:** This research received no external funding. Heidelberg University helped to bridge critical periods.

**Institutional Review Board Statement:** Not applicable.

**Informed Consent Statement:** Not applicable.

**Data Availability Statement:** All relevant data will become publicly available with the publication of the PhD thesis of the first author at Heidelberg University.

**Acknowledgments:** The authors would like to express their gratitude to Henk Thoma (Leh, Ladakh, India) for the continuous and generous support over many years. The German Aerospace Center (DLR) kindly provided TanDEM-X data and the Swiss Organisation WSL kindly provided the Mono-plotting Tool. Constructive comments by two anonymous reviewers helped to improve the article.

**Conflicts of Interest:** The authors declare no conflict of interest.



Table A2. Cont.

	Jan	Feb	Mar	Apr	May	Jun	Jul	Aug	Sep	Oct	Nov	Dec	Aut.	Win.	Spr.	Sum.	Ann.
<b>Tshomoriri</b>																	
<b>Z-Value</b>	−0.35	0.14	1.05	0.00	0.35	0.84	1.89	0.56	0.63	−0.42	−0.49	−0.63	−0.14	−0.07	0.56	1.19	0.35
<b>p-Value</b>	0.73	0.89	0.29	1.00	0.73	0.40	<b>0.06</b>	0.58	0.53	0.67	0.62	0.53	0.89	0.94	0.58	0.23	0.73
<b>Sen's S.</b>	−0.35	0.26	0.68	−0.07	0.21	0.31	0.25	0.07	0.14	−0.27	−0.23	−0.41	−0.03	−0.09	0.32	0.18	0.13
<b>Lin. S.</b>	−0.20	0.37	0.59	0.19	0.28	0.37	0.28	0.06	−0.09	0.22	0.17	−0.23	0.12	−0.02	0.35	0.24	0.17
<b>Mean</b>	61.27	75.13	73.45	61.13	34.05	14.70	6.34	6.21	12.02	17.67	21.60	33.72	17.18	56.71	56.21	9.08	34.77
<b>SD</b>	21.21	17.34	18.27	16.11	13.45	7.73	4.04	2.51	11.39	18.02	16.77	19.15	14.25	13.09	14.55	3.92	8.42
<b>Trend</b>	↓	↑	↑	↓	↑	↑	↑	↑	↑	↓	↓	↓	↓	↓	↑	↑	↑
<b>Zangskar</b>																	
<b>Z-Value</b>	−0.35	0.70	0.63	0.49	0.42	1.54	2.03	1.33	0.63	0.00	0.21	−0.07	0.00	0.21	0.42	1.68	0.77
<b>p-Value</b>	0.73	0.48	0.53	0.62	0.67	0.12	<b>0.04</b>	0.18	0.53	1.00	0.83	0.94	1.00	0.83	0.67	<b>0.09</b>	0.44
<b>Sen's S.</b>	−0.31	0.20	0.17	0.21	0.22	0.63	0.37	0.09	0.12	0.12	0.10	−0.03	0.02	0.15	0.13	0.28	0.26
<b>Lin. S.</b>	0.16	0.38	0.24	0.19	0.19	0.56	0.35	0.18	0.11	0.59	0.24	0.01	0.28	0.18	0.21	0.36	0.27
<b>Mean</b>	72.93	80.89	82.44	72.05	49.89	26.37	11.61	8.34	15.65	24.62	37.46	52.50	26.10	68.77	68.13	15.44	44.56
<b>SD</b>	12.25	8.87	8.61	10.57	8.65	8.81	4.58	2.58	7.20	14.77	14.97	18.66	9.72	8.53	8.53	4.93	5.90
<b>Trend</b>	↓	↑	↑	↑	↑	↑	↑	↑	↑	↑	↑	↓	↑	↑	↑	↑	↑

Numbers in bold and green: significance level,  $p$ -value < 0.1. Numbers in bold and blue: significance level,  $p$ -value < 0.05.

Table A3. Trend analysis of SCA in relation to the elevation zone (%) of all subregions.

Elevation Zone	Region	Jan	Feb	Mar	Apr	May	Jun	Jul	Aug	Sep	Oct	Nov	Dec
<3500 m	Siachan	▽	▽	▲	▲	▲	▲	▲	▲	▲	▽	▲	▲
	Shayok	▲	▲	▲	▲	▲	▲	▲	▲*	▽	▲	▲	▽
	Indus	▽	▲	▲	▲	▲	▲	▲	▲	▲	▲	▲	▲
	Suru	▲	▲	▲	▲	▲	▲	▲	▲	▲	▽	▽	▽
	Zangskar	▽*	▲	▲	▲	▲	▲	▽	▽	▽	▲	▽	▽
3500–4500 m	Siachan	▲	▽	▲	▲	▲	▲	▲	▲	▲	▲	▲	▲
	Shayok	▲	▲	▽	▲	▲	▲	▲	▲	▲	▲	▲	▲
	Pangong	▲	▲	▲	▲	▲*	▲*	▲*	▲*	▲*	▽	▲	▲
	Indus	▽	▲	▲	▲	▲	▲	▲	▲	▲	▲	▲	▲
	Suru	▲	▲	▽	▲	▲	▲	▲	▲	▲	▲	▲	▲
	Zangskar	▽	▲	▲	▲	▲	▲	▲	▲	▲	▲	▲	▲
4500–5500 m	Siachan	▲	▽	▲	▲	▲	▲	▲	▲	▲	▽	▲	▽
	Shayok	▽	▲	▽*	▽	▽	▲*	▲	▲	▲	▲	▲	▽
	Pangong	▽	▲	▲	▲*	▽	▲	▲	▽	▲	▽	▽	▽
	Indus	▽	▲	▲	▲	▽	▲	▲	▲	▲	▲	▲	▲
	Suru	▲	▽	▽	▲	▲	▲	▲	▲	▲	▲	▲	▲
	Zangskar	▽	▲	▲	▲	▲	▲	▲	▲	▲	▲	▲	▲
5500–6500 m	Siachan	▲	▽	▽	▽	▽*	▽*	▲	▽	▽	▲	▽	▽
	Shayok	▽	▽	▲*	▲*	▲*	▲*	▲	▽	▽	▲	▲	▽
	Pangong	▽	▽	▽	▽	▽	▽*	▲	▽*	▲	▽	▽	▽
	Indus	▽	▲	▽	▲*	▽	▽*	▲	▲	▲	▽	▲	▽
	Suru	▲	▽	▲*	▲*	▽*	▽*	▲	▲	▲	▲	▲	▲
	Zangskar	▽	▲	▲	▲	▽	▽	▲	▲	▲	▲	▲	▲
>6500 m	Siachan	▽	▲*	▽	—	▲*	▲*	▲*	▲*	▲*	▽*	▽	▽
	Shayok	—	—*	—	—	—	▲*	—	▽	—	—	—	—
	Indus	—	—	—	—	—	▲*	▲*	▲*	—	—	—	—
	Suru	▲*	—*	▲*	▲*	—*	▲*	—	▲*	▲*	▲*	▲*	—
	Zangskar	—	—	—	—	—	—	—	—	—	—	—	—
	Tshomoriri	—	—	—	—	—	—	—	▲*	▲*	—	—	—

△ Upward Trend, ▽ Downward Trend, — No Trend; Trend Significance: ▲ None ▲ Low ( $p < 0.1$ ) ▲ Moderate ( $p < 0.05$ ) ▲ High ( $p < 0.01$ ), \* Modified Mann-Kendall Test.

## References

1. Armstrong, R.L.; Rittger, K.; Brodzik, M.J.; Racoviteanu, A.; Barrett, A.P.; Khalsa, S.-J.S.; Raup, B.; Hill, A.F.; Khan, A.L.; Wilson, A.M.; et al. Runoff from Glacier Ice and Seasonal Snow in High Asia: Separating Melt Water Sources in River Flow. *Reg. Environ. Chang.* **2019**, *19*, 1249–1261. [\[CrossRef\]](#)
2. Jain, S.K.; Goswami, A.; Saraf, A. Role of Elevation and Aspect in Snow Distribution in Western Himalaya. *Water Resour. Manag.* **2009**, *23*, 71–83. [\[CrossRef\]](#)
3. Misra, A.; Kumar, A.; Bhambri, R.; Haritashya, U.K.; Verma, A.; Dobhal, D.P.; Gupta, A.K.; Gupta, G.; Upadhyay, R. Topographic and Climatic Influence on Seasonal Snow Cover: Implications for the Hydrology of Ungauged Himalayan Basins, India. *J. Hydrol.* **2020**, *585*, 124716. [\[CrossRef\]](#)
4. Mukherji, A.; Molden, D.; Nepal, S.; Rasul, G.; Wagnon, P. Himalayan Waters at the Crossroads: Issues and Challenges. *Int. J. Water Resour. Dev.* **2015**, *31*, 151–160. [\[CrossRef\]](#)
5. Mukherji, A.; Sinisalo, A.; Nüsser, M.; Garrard, R.; Eriksson, M. Contributions of the Cryosphere to Mountain Communities in the Hindu Kush Himalaya: A Review. *Reg. Environ. Chang.* **2019**, *19*, 1311–1326. [\[CrossRef\]](#)
6. Nüsser, M.; Dame, J.; Parveen, S.; Kraus, B.; Baghel, R.; Schmidt, S. Cryosphere-Fed Irrigation Networks in the Northwestern Himalaya: Precarious Livelihoods and Adaptation Strategies Under the Impact of Climate Change. *Mt. Res. Dev.* **2019**, *39*, R1–R11. [\[CrossRef\]](#)
7. Nüsser, M.; Schmidt, S.; Dame, J. Irrigation and Development in the Upper Indus Basin: Characteristics and Recent Changes of a Socio-Hydrological System in Central Ladakh, India. *Mt. Res. Dev.* **2012**, *32*, 51–61. [\[CrossRef\]](#)
8. Hock, R.; Rasul, G.; Adler, C.; Cáceres, B.; Gruber, S.; Hirabayashi, Y.; Jackson, M.; Käab, A.; Kang, S.; Kutuzov, S.; et al. High Mountain Areas. In *IPCC Special Report on the Ocean and Cryosphere in a Changing Climate*; Cambridge University Press: Cambridge, UK, 2019; pp. 131–202.
9. Barnett, T.P.; Adam, J.C.; Lettenmaier, D.P. Potential Impacts of a Warming Climate on Water Availability in Snow-Dominated Regions. *Nature* **2005**, *438*, 303–309. [\[CrossRef\]](#)
10. Nüsser, M.; Dame, J.; Kraus, B.; Baghel, R.; Schmidt, S. Socio-Hydrology of “Artificial Glaciers” in Ladakh, India: Assessing Adaptive Strategies in a Changing Cryosphere. *Reg. Environ. Chang.* **2019**, *19*, 1327–1337. [\[CrossRef\]](#)
11. Winiger, M.; Gumpert, M.; Yamout, H. Karakorum–Hindukush–Western Himalaya: Assessing High-Altitude Water Resources. *Hydrol. Process.* **2005**, *19*, 2329–2338. [\[CrossRef\]](#)
12. Dharpure, J.K.; Goswami, A.; Patel, A.; Kulkarni, A.V.; Snehmani. Assessment of Snow Cover Variability and Its Sensitivity to Hydrometeorological Factors in the Karakoram and Himalayan Region. *Hydrol. Sci. J.* **2021**, *66*, 2198–2215. [\[CrossRef\]](#)
13. Immerzeel, W.W.; Droogers, P.; de Jong, S.M.; Bierkens, M.F.P. Large-Scale Monitoring of Snow Cover and Runoff Simulation in Himalayan River Basins Using Remote Sensing. *Remote Sens. Environ.* **2009**, *113*, 40–49. [\[CrossRef\]](#)
14. Muhammad, S.; Thapa, A. Daily Terra–Aqua MODIS Cloud-Free Snow and Randolph Glacier Inventory 6.0 Combined Product (M\* D10A1GL06) for High-Mountain Asia between 2002 and 2019. *Earth Syst. Sci. Data* **2021**, *13*, 767–776. [\[CrossRef\]](#)
15. Salzmann, N.; Huggel, C.; Rohrer, M.; Stoffel, M. Data and Knowledge Gaps in Glacier, Snow and Related Runoff Research—A Climate Change Adaptation Perspective. *J. Hydrol.* **2014**, *518*, 225–234. [\[CrossRef\]](#)
16. Gusain, H.; Mishra, V.; Bhutiyani, M. Winter Temperature and Snowfall Trends in the Cryospheric Region of North-West Himalaya. *Mausam* **2014**, *65*, 425–432. [\[CrossRef\]](#)
17. Ahmad, I.; Ahmad, Z.; Munir, S.; Shah, S.R.A.; Shabbir, Y. Geo-Spatial Dynamics of Snowcover and Hydro Meteorological Parameters of Astore Basin, UIB, HKH Region, Pakistan. *Arab. J. Geosci.* **2018**, *11*, 419. [\[CrossRef\]](#)
18. Bilal, H.; Chamhuri, S.; Mokhtar, M.B.; Kanniah, K.D. Recent Snow Cover Variation in the Upper Indus Basin of Gilgit Baltistan, Hindukush Karakoram Himalaya. *J. Mt. Sci.* **2019**, *16*, 296–308. [\[CrossRef\]](#)
19. Dai, L.; Che, T.; Ding, Y.; Hao, X. Evaluation of Snow Cover and Snow Depth on the Qinghai-Tibetan Plateau Derived from Passive Microwave Remote Sensing. *Cryosphere* **2017**, *11*, 1933–1948. [\[CrossRef\]](#)
20. Saydi, M.; Ding, J. Impacts of Topographic Factors on Regional Snow Cover Characteristics. *Water Sci. Eng.* **2020**, *13*, 171–180. [\[CrossRef\]](#)
21. Sood, V.; Singh, S.; Taloor, A.K.; Prashar, S.; Kaur, R. Monitoring and Mapping of Snow Cover Variability Using Topographically Derived NDSI Model over North Indian Himalayas during the Period 2008–19. *Appl. Comput. Geosci.* **2020**, *8*, 100040. [\[CrossRef\]](#)
22. Schmidt, S.; Weber, B.; Winiger, M. Analyses of Seasonal Snow Disappearance in an Alpine Valley from Micro- to Meso-Scale (Loetschental, Switzerland). *Hydrol. Process.* **2009**, *23*, 1041–1051. [\[CrossRef\]](#)
23. McKay, G.A.; Gray, D.M. The Distribution of Snowcover. In *Handbook of Snow. Principles, Processes, Management & Use*; Gray, D.M., Male, D.H., Eds.; Pergamon Press: Oxford, UK, 1981; pp. 153–190.
24. Sahu, R.; Gupta, R.D. Snow Cover Area Analysis and Its Relation with Climate Variability in Chandra Basin, Western Himalaya, during 2001–2017 Using MODIS and ERA5 Data. *Environ. Monit. Assess.* **2020**, *192*, 489. [\[CrossRef\]](#) [\[PubMed\]](#)
25. Dahri, Z.H.; Ludwig, F.; Moors, E.; Ahmad, B.; Khan, A.; Kabat, P. An Appraisal of Precipitation Distribution in the High-Altitude Catchments of the Indus Basin. *Sci. Total Environ.* **2016**, *548–549*, 289–306. [\[CrossRef\]](#) [\[PubMed\]](#)
26. Norman, R.; Thoma, H. *Rang-Skat. A Ladakhi-English Dictionary*; Melong Publications: Leh, India, 2019.
27. Schmidt, S.; Nüsser, M. Changes of High Altitude Glaciers in the Trans-Himalaya of Ladakh over the Past Five Decades (1969–2016). *Geosciences* **2017**, *7*, 27. [\[CrossRef\]](#)

28. Schmidt, S.; Nüsser, M. Changes of High Altitude Glaciers from 1969 to 2010 in the Trans-Himalayan Kang Yatze Massif, Ladakh, Northwest India. *Arct. Antarct. Alp. Res.* **2012**, *44*, 107–121. [[CrossRef](#)]
29. Soheb, M.; Ramanathan, A.; Bhardwaj, A.; Sam, L. Spatiotemporal Quantification of Key Environmental Changes in Stok and Kang Yatze Regions of Ladakh Himalaya, India. *Geocarto Int.* **2022**, 1–22. [[CrossRef](#)]
30. Soheb, M.; Ramanathan, A.; Angchuk, T.; Mandal, A.; Kumar, N.; Lotus, S. Mass-Balance Observation, Reconstruction and Sensitivity of Stok Glacier, Ladakh Region, India, between 1978 and 2019. *J. Glaciol.* **2020**, *66*, 627–642. [[CrossRef](#)]
31. Bhambri, R.; Bolch, T.; Kawishwar, P.; Dobhal, D.; Srivastava, D.; Pratap, B. Heterogeneity in Glacier Response in the Upper Shyok Valley, Northeast Karakoram. *Cryosphere* **2013**, *7*, 1385–1398. [[CrossRef](#)]
32. Bhutiyani, M. Mass-Balance Studies on Siachen Glacier in the Nubra Valley, Karakoram Himalaya, India. *J. Glaciol.* **1999**, *45*, 112–118. [[CrossRef](#)]
33. Kamp, U.; Byrne, M.; Bolch, T. Glacier Fluctuations between 1975 and 2008 in the Greater Himalaya Range of Zaskar, Southern Ladakh. *J. Mt. Sci.* **2011**, *8*, 374–389. [[CrossRef](#)]
34. Brombierstäudl, D.; Schmidt, S.; Nüsser, M. Distribution and Relevance of Aufeis (Icing) in the Upper Indus Basin. *Sci. Total Environ.* **2021**, *780*, 146604. [[CrossRef](#)] [[PubMed](#)]
35. Pfister, O. *Birds and Mammals of Ladakh*; Oxford University Press: Oxford, UK, 2004.
36. Riggs, G.A.; Hall, D.K.; Salomonson, V.V. MODIS Snow Products User Guide to Collection 5. *Digit. Media* **2006**, *80*, 1–80.
37. Shean, D. *High Mountain Asia 8-Meter DEM Mosaics Derived from Optical Imagery*; Version 1; NASA National Snow and Ice Data Center Distributed Active Archive Center: Boulder, CO, USA, 2017.
38. Riggs, G.A.; Hall, D.K.; Román, M.O. *MODIS Snow Products Collection 6 User Guide*; National Snow and Ice Data Center: Boulder, CO, USA, 2015; 66p.
39. Zhang, H.; Zhang, F.; Zhang, G.; Che, T.; Yan, W.; Ye, M.; Ma, N. Ground-Based Evaluation of MODIS Snow Cover Product V6 across China: Implications for the Selection of NDSI Threshold. *Sci. Total Environ.* **2019**, *651*, 2712–2726. [[CrossRef](#)] [[PubMed](#)]
40. Jain, S.K.; Goswami, A.; Saraf, A.K. Accuracy Assessment of MODIS, NOAA and IRS Data in Snow Cover Mapping under Himalayan Conditions. *Int. J. Remote Sens.* **2008**, *29*, 5863–5878. [[CrossRef](#)]
41. Singh, S.K.; Rathore, B.P.; Bahuguna, I.M.; Ajai. Snow Cover Variability in the Himalayan-Tibetan Region: Snow cover in Himalayan-Tibetan region. *Int. J. Climatol.* **2014**, *34*, 446–452. [[CrossRef](#)]
42. Kulkarni, A.V.; Rathore, B.P.; Singh, S.K.; Ajai. Distribution of seasonal snow cover in central and western Himalaya. *Ann. Glaciol.* **2010**, *51*, 123–128. [[CrossRef](#)]
43. Zhang, Y.; Yan, S.; Lu, Y. Snow Cover Monitoring Using MODIS Data in Liaoning Province, Northeastern China. *Remote Sens.* **2010**, *2*, 777–793. [[CrossRef](#)]
44. Hall, D.K.; Riggs, G.A.; Salomonson, V.V.; Barton, J.; Casey, K.; Chien, J.; DiGirolamo, N.; Klein, A.; Powell, H.; Tait, A. *Algorithm Theoretical Basis Document (ATBD) for the MODIS Snow and Sea Ice-Mapping Algorithms*; NASA GSFC: Greenbelt, MD, USA, 2001; 45p.
45. Salomonson, V.V.; Appel, I. Estimating Fractional Snow Cover from MODIS Using the Normalized Difference Snow Index. *Remote Sens. Environ.* **2004**, *89*, 351–360. [[CrossRef](#)]
46. Tran, H.; Nguyen, P.; Ombadi, M.; Hsu, K.; Sorooshian, S.; Qing, X. A Cloud-Free MODIS Snow Cover Dataset for the Contiguous United States from 2000 to 2017. *Sci. Data* **2019**, *6*, 180300. [[CrossRef](#)]
47. Zhang, Y.; Cao, T.; Kan, X.; Wang, J.; Tian, W. Spatial and Temporal Variation Analysis of Snow Cover Using MODIS over Qinghai-Tibetan Plateau during 2003–2014. *J. Indian Soc. Remote Sens.* **2017**, *45*, 887–897. [[CrossRef](#)]
48. Chokmani, K.; Dever, K.; Bernier, M.; Gauthier, Y.; Paquet, L.-M. Adaptation of the SNOWMAP Algorithm for Snow Mapping over Eastern Canada Using Landsat-TM Imagery. *Hydrol. Sci. J.* **2010**, *55*, 649–660. [[CrossRef](#)]
49. Hall, D.K.; Riggs, G.A.; Salomonson, V.V.; DiGirolamo, N.E.; Bayr, K.J. MODIS Snow-Cover Products. *Remote Sens. Environ.* **2002**, *83*, 181–194. [[CrossRef](#)]
50. Hall, D.K.; Riggs, G.A.; Salomonson, V.V. Development of Methods for Mapping Global Snow Cover Using Moderate Resolution Imaging Spectroradiometer Data. *Remote Sens. Environ.* **1995**, *54*, 127–140. [[CrossRef](#)]
51. Cohen, J. A Coefficient of Agreement for Nominal Scales. *Educ. Psychol. Meas.* **1960**, *20*, 37–46. [[CrossRef](#)]
52. Hall, D.K.; Riggs, G.A. Accuracy Assessment of the MODIS Snow Products. *Hydrol. Process.* **2007**, *21*, 1534–1547. [[CrossRef](#)]
53. López-Burgos, V.; Gupta, H.V.; Clark, M. Reducing Cloud Obscuration of MODIS Snow Cover Area Products by Combining Spatio-Temporal Techniques with a Probability of Snow Approach. *Hydrol. Earth Syst. Sci.* **2013**, *17*, 1809–1823. [[CrossRef](#)]
54. Parajka, J.; Pepe, M.; Rampini, A.; Rossi, S.; Blöschl, G. A Regional Snow-Line Method for Estimating Snow Cover from MODIS during Cloud Cover. *J. Hydrol.* **2010**, *381*, 203–212. [[CrossRef](#)]
55. Parajka, J.; Blöschl, G. Spatio-Temporal Combination of MODIS Images—Potential for Snow Cover Mapping. *Water Resour. Res.* **2008**, *44*, W03406. [[CrossRef](#)]
56. Gafurov, A.; Bárdossy, A. Cloud Removal Methodology from MODIS Snow Cover Product. *Hydrol. Earth Syst. Sci.* **2009**, *13*, 1361–1373. [[CrossRef](#)]
57. Gao, Y.; Xie, H.; Yao, T.; Xue, C. Integrated Assessment on Multi-Temporal and Multi-Sensor Combinations for Reducing Cloud Obscuration of MODIS Snow Cover Products of the Pacific Northwest USA. *Remote Sens. Environ.* **2010**, *114*, 1662–1675. [[CrossRef](#)]
58. Paudel, K.P.; Andersen, P. Monitoring Snow Cover Variability in an Agropastoral Area in the Trans Himalayan Region of Nepal Using MODIS Data with Improved Cloud Removal Methodology. *Remote Sens. Environ.* **2011**, *115*, 1234–1246. [[CrossRef](#)]

59. Hauksson, B.P. Estimation of Regional Snow-Line Elevations in Norway. Testing a Method for Estimating RSLE and Melt Slope Analysis in Norway. Master's Thesis, University of Oslo, Oslo, Norway, 2017.
60. Krajčí, P.; Holko, L.; Perdigão, R.A.; Parajka, J. Estimation of Regional Snowline Elevation (RSLE) from MODIS Images for Seasonally Snow Covered Mountain Basins. *J. Hydrol.* **2014**, *519*, 1769–1778. [[CrossRef](#)]
61. Kendall, M. *Rank Correlation Methods*; Charles Griffin: London, UK, 1975.
62. Mann, H.B. Nonparametric Tests against Trend. *Econom. J. Econom. Soc.* **1945**, *13*, 245–259. [[CrossRef](#)]
63. Sen, P.K. Estimates of the Regression Coefficient Based on Kendall's Tau. *J. Am. Stat. Assoc.* **1968**, *63*, 1379–1389. [[CrossRef](#)]
64. Hamed, K.H.; Rao, A.R. A Modified Mann-Kendall Trend Test for Autocorrelated Data. *J. Hydrol.* **1998**, *204*, 182–196. [[CrossRef](#)]
65. Yue, S.; Wang, C. The Mann-Kendall Test Modified by Effective Sample Size to Detect Trend in Serially Correlated Hydrological Series. *Water Resour. Manag.* **2004**, *18*, 201–218. [[CrossRef](#)]
66. Gascoin, S.; Hagolle, O.; Huc, M.; Jarlan, L.; Dejoux, J.-F.; Szczypta, C.; Marti, R.; Sánchez, R. A Snow Cover Climatology for the Pyrenees from MODIS Snow Products. *Hydrol. Earth Syst. Sci.* **2015**, *19*, 2337–2351. [[CrossRef](#)]
67. Klein, A.G.; Barnett, A.C. Validation of Daily MODIS Snow Cover Maps of the Upper Rio Grande River Basin for the 2000–2001 Snow Year. *Remote Sens. Environ.* **2003**, *86*, 162–176. [[CrossRef](#)]
68. Liang, T.G.; Huang, X.D.; Wu, C.X.; Liu, X.Y.; Li, W.L.; Guo, Z.G.; Ren, J.Z. An Application of MODIS Data to Snow Cover Monitoring in a Pastoral Area: A Case Study in Northern Xinjiang, China. *Remote Sens. Environ.* **2008**, *112*, 1514–1526. [[CrossRef](#)]
69. Zhang, Y.; Kan, X.; Ren, W.; Cao, T.; Tian, W.; Wang, J. Snow Cover Monitoring in Qinghai-Tibetan Plateau Based on Chinese Fengyun-3/VIRR Data. *J. Indian Soc. Remote Sens.* **2017**, *45*, 271–283. [[CrossRef](#)]
70. Girona-Mata, M.; Miles, E.S.; Ragetti, S.; Pellicciotti, F. High-Resolution Snowline Delineation from Landsat Imagery to Infer Snow Cover Controls in a Himalayan Catchment. *Water Resour. Res.* **2019**, *55*, 6754–6772. [[CrossRef](#)]
71. Aschenwald, J.; Leichter, K.; Tasser, E.; Tappeiner, U. Spatio-Temporal Landscape Analysis in Mountainous Terrain by Means of Small Format Photography: A Methodological Approach. *IEEE Trans. Geosci. Remote Sens.* **2001**, *39*, 885–893. [[CrossRef](#)]
72. Corripio, J. Snow Surface Albedo Estimation Using Terrestrial Photography. *Int. J. Remote Sens.* **2004**, *25*, 5705–5729. [[CrossRef](#)]
73. Tahir, A.A.; Chevallier, P.; Arnaud, Y.; Ashraf, M.; Bhatti, M.T. Snow Cover Trend and Hydrological Characteristics of the Astore River Basin (Western Himalayas) and Its Comparison to the Hunza Basin (Karakoram Region). *Sci. Total Environ.* **2015**, *505*, 748–761. [[CrossRef](#)] [[PubMed](#)]
74. Hasson, S.; Lucarini, V.; Khan, M.R.; Petitta, M.; Bolch, T.; Gioli, G. Early 21st Century Snow Cover State over the Western River Basins of the Indus River System. *Hydrol. Earth Syst. Sci.* **2014**, *18*, 4077–4100. [[CrossRef](#)]
75. Mieke, G.; Winiger, M.; Böhner, J.; Yili, Z. The Climatic Diagram Map of High Asia. *Erdkunde* **2001**, *55*, 94–98. [[CrossRef](#)]
76. Dimri, A.P.; Chevuturi, A. Model Sensitivity Analysis Study for Western Disturbances over the Himalayas. *Meteorol. Atmos. Phys.* **2014**, *123*, 155–180. [[CrossRef](#)]
77. Gurung, D.R.; Maharjan, S.B.; Shrestha, A.B.; Singh Shrestha, M.; Bajracharya, S.R.; Murthy, M.S.R. Climate and Topographic Controls on Snow Cover Dynamics in the Hindu Kush Himalaya. *Int. J. Climatol.* **2017**, *37*, 3873–3882. [[CrossRef](#)]
78. Richter, M. Klimatologische und pflanzenmorphologische Vertikalgradienten in Hochgebirgen. *Erdkunde* **1996**, *50*, 205–237. [[CrossRef](#)]
79. Nüsser, M.; Baghel, R. The Emergence of the Cryoscape: Contested Narratives of Himalayan Glacier Dynamics and Climate Change. In *Environmental and Climate Change in South and Southeast Asia*; Schuler, B., Ed.; Brill: Leiden, The Netherlands, 2014; pp. 138–156.